Joint International Topical Meeting on Mathematics & Computation and Supercomputing in Nuclear Applications (M&C + SNA 2007)
Monterey, California, April 15-19, 2007, on CD-ROM, American Nuclear Society, LaGrange Park, IL (2007)

WAVE PROPAGATION ALGORITHMS AND ADAPTIVE MESH REFINEMENT FOR CFD SIMULATIONS OF POTENTIAL HYDROGEN EXPLOSIONS IN NUCLEAR CONTAINMENT STRUCTURES

D. Calhoun and H. Paillère
Commissariat à l'Énergie Atomique
DM2S/SFME/LTMF Bt. 454
Centre de Saclay
91191, Gif-sur-Yvette, France
donna.calhoun@cea.fr, henri.paillere@cea.fr

ABSTRACT

We present a high resolution, finite-volume Cartesian grid method for simulating potential explosions in nuclear containment structures. The basic method is a Godunov-type method that relies on the solution to non-linear Riemann problems at the interfaces between cells of a uniform Cartesian mesh. We have extended these methods to general quadrilateral and hexahedral adaptively refined grids. Two- and three-dimensional results are presented for a simplified combustion problem in a nuclear containment facility.

Key words : High resolution, finite-volume schemes, adaptive-mesh refinement, curvilinear grids, logically Cartesian grids, hydrogen detonation, nuclear safety, nuclear containment structures.

1 INTRODUCTION

In the event of a Loss of Coolant Accident (LOCA) in a Pressurized Water Reactor, hydrogen may be produced in the reactor core by the reactor between steam and the fuel cladding, and released through the breach into the containment. Thus, in a severe accident, the atmosphere of the containment may contain air, steam and hydrogen, potentially forming combustible mixtures. In the Three Mile accident on March 28, 1979, about 450kg of H2 were thus formed and released into the containment, and later burned in a mild deflagration. Following the TMI accident, specific mitigation devices (ignitors, recombiners) to control the concentration levels of H2 were introduced, and have been installed in most existing plants, and or incorporated in the design of the new generation of reactors. From a safety analysis point of view, it is now required from operators or vendors to demonstrate the adequacy of the H2 control measures, since the most severe hydrogen combustion regimes (fast deflagrations, detonations) could potentially threaten the integrity of the containment.

For this reason, it is important to be able to accurately predict any potential damage that may occur in the event of an explosion and to design appropriate mitigation measures (such as recombiners to remove H2). To predict the stresses that may result from potential blast loading on the containment structure, one must

be able to obtain precise estimates of both the spatial and temporal multi-dimensional dynamics of the explosion itself [1]. In what follows, we present prelimary results from research aimed at solving the full two- and three-dimensional equations of reactive gas dynamics in a realistic geometry relevant to the problem of studying potential explosions in containments.

The finite-volume methods we use for this numerical study are based on the wave propagation algorithms developed by R. LeVeque and described in detail in [10]. These methods are developed for structured uniform finite-volume grids, but we have extended them to mapped two- and three-dimensional grids. To model peak over-pressures precisely, we use adaptively refined meshes to dynamically capture the formation of pressure peaks and track accurately their transient behavior.

2 REACTIVE EULER EQUATIONS

We focus our attention on the equations of reactive gas-dynamics given by

$$\partial_t \mathbf{q} + \nabla \cdot \mathbf{f}(\mathbf{q}) = S(\mathbf{q}, \ldots) \tag{1}$$

where $\mathbf{q}$ is a vector of conserved quantities given by $\mathbf{q} = (\rho, \mathbf{u}\rho, E, \rho Z)$ consisting of the density $\rho(\mathbf{x}, t)$, velocity field $\mathbf{u} = (u(\mathbf{x}, t), v(\mathbf{x}, t), w(\mathbf{x}, t))$, total energy $E(\mathbf{x}, t)$, and the progress variable $Z(\mathbf{x}, t)$. In unburned regions, $Z = 1$, and in burned regions, $Z = 0$. We use $\mathbf{x}$ to denote the two- or three-dimensional spatial location.

The flux function $\mathbf{f}(\mathbf{q})$ is given in three dimensions as

$$\mathbf{f}(\mathbf{q}) = \begin{pmatrix} \rho u & \rho v & \rho w \\ \rho u^2 + p & \rho v u & \rho w u \\ \rho u v & \rho v^2 + p & \rho w v \\ \rho u w & \rho v w & \rho w^2 + p \\ u(E+p) & v(E+p) & w(E+p) \\ u\rho Z & v\rho Z & w\rho Z \end{pmatrix} \tag{2}$$

where $p(\mathbf{x}, t)$ is the pressure.

The source term $S(\mathbf{q}, \ldots)$ is the vector $(0, 0, 0, 0, 0, \Psi(\mathbf{q}, \ldots))$ and models the reaction. The physical model we use assumes that reactants are converted into products in a single step. The particular form that the source term Ψ takes will depend on whether we wish to model deflagration or detonation. To model detonations, we use a simplified Arrhenius law given by

$$\Psi(Z(\mathbf{x}, t)) = \begin{cases} -\dfrac{1}{\tau} Z(\mathbf{x}, t), & T(\mathbf{x}, t) \geq T_{ign} \\ 0 & \text{otherwise} \end{cases} \tag{3}$$

where $T(\mathbf{x}, t)$ is the temperature of the gas, determined using an ideal gas law. For deflagrations, we use the CREBCOM model [8], given approximately by

$$\Psi(Z(\mathbf{x}, t)) = -K\delta(\mathbf{x} - \alpha(Z(\mathbf{x}, t))) \tag{4}$$

where $\delta(Z(\mathbf{x},t))$ is a Dirac delta function. The location $\alpha(Z(\mathbf{x},t))$ of the burning front is determined by looking for steep gradients in the variable Z.

The general equation of state needed to close the system is given by

$$E = -p + \rho\left(h_0 + \int_{T_0}^{T} c_p(\tau; Z)\, d\tau\right) + \frac{1}{2}\rho(u^2 + v^2 + w^2) \tag{5}$$

where again, $T(\mathbf{x},t)$ is the temperature of the gas, and $h_0 = h(T_0)$ is the specific enthalpy at a reference temperature T_0. In general, the heat capacity c_p depends on temperature and the state Z. For the present work, however, we assume that the gas is calorically perfect (i.e. c_p is independent of temperature), and so the equation of state reduces to that for a polytropic gas and is given by

$$E = \frac{p}{\gamma - 1} + \frac{1}{2}\rho(u^2 + v^2 + w^2) + \rho Q Z \tag{6}$$

where Q is the energy released upon conversion of reactants to products. We set the adiabatic exponent γ to 1.4.

3 A WAVE PROPAGATION APPROACH TO SOLVING HYPERBOLIC CONSERVATION LAWS

A standard way to solve the system in (1) is to use a finite-volume, Godunov-type scheme. Such schemes require that the system be in conservation form, i.e. written in terms of a flux function. In what follows, we first give a brief overview of the Godunov approach for a one-dimensional conservation law. Then we describe in more detail a related approach, the wave propagation algorithm.

To begin, we consider a system of hyperbolic conservation laws in one spatial dimension given by

$$\mathbf{q}_t + f(\mathbf{q})_x = 0 \tag{7}$$

We discretize a one-dimensional grid at cell centers $x_i = a + (i - 1/2)\Delta x$ for $i = 1, \ldots N$ where a is the left edge of our domain, and Δx is the uniform mesh spacing. Our finite-volume cell C_i is the cell $[x_{i-1/2}, x_{i+1/2}]$ with cell center is x_i and faces$x_{i-1/2}$ and $x_{i+1/2}$. We denote discrete time levels using $t_n = n\Delta t$, where the time step Δt is chosen to respect the CFL condition. In a finite-volume scheme, we solve for cell-averaged values Q_i^n, defined as

$$Q_i^n \equiv \frac{1}{\Delta x}\int_{x_{i-1/2}}^{x_{i+1/2}} \mathbf{q}(x, t_n)\, dx. \tag{8}$$

A typical finite-volume update for the equation given in (7) is then

$$Q_i^{n+1} = Q_i^n - \frac{\Delta t}{\Delta x}\left(F_{i+1/2}^n - F_{i-1/2}^n\right) \tag{9}$$

where the numerical fluxes $F^n_{i-1/2}$ are the approximations

$$F^n_{i-1/2} \approx \frac{1}{\Delta t}\int_{t_n}^{t_{n+1}} \mathbf{f}(\mathbf{q}(x_{i-1/2},t))\, dt. \tag{10}$$

The central idea in Godunov's scheme is to use the solution q^* to a Riemann problem in place of $\mathbf{q}(x_{i-1/2},t)$ in the integral above. A typical Riemann problem is given by the one-dimensional conservation law in (7) along with a special set of initial conditions given by

$$\mathbf{q}(x,0)\begin{cases} \mathbf{q}_l & x<0 \\ \mathbf{q}_r & x>0 \end{cases} \tag{11}$$

where q_l and q_r are constant values. For the Euler equations, one can solve the non-linear problem analytically to obtain an exact solution to the Riemann problem. However, it is often acceptable to use an approximate solver. For details on solving Riemann problems, see [10, 13]. In the standard Godunov scheme, one solves Riemann problems at each cell interface $x_{i-1/2}$ using left state $\mathbf{q}_l = Q^n_{i-1}$ and right state $\mathbf{q}_r = Q^n_i$ to obtain the solution $\mathbf{q}^*(Q^n_{i-1}, Q^n_i)$. This solution, assumed to be constant over the interval $[t_n\ , t_{n+1}\ ]$ is used in place of $\mathbf{q}(x_{i-1/2},t)$ in (10) and the resulting numerical fluxes are used in (9). The resulting scheme is the well-known first order Godunov scheme and has the advantage that it is conservative and captures shocks and rarefactions well. Moreover, it is stable up to Courant number 1.

3.1 The wave propagation approach

This standard approach, however, assumes that our hyperbolic probem is given in conservation form and that we have a flux function available. This excludes some very common systems of hyperbolic equations, such as a scalar advection equation, linear acoustics equation with variable coefficients, or species transport. In general, such equations are typically in linear or quasi-linear form, given by

$$\mathbf{q}_t + \mathbf{A}\mathbf{q}_x = 0 \tag{12}$$

where $A \in R^{m\times m}$ may depend on $\mathbf{q}$ or the spatial location. Moreoever, systems written in conservative form may also be written in quasi-linear form, and in fact, this form is needed to obtain characteristic information about the system. A quasi-linear form for system (1) is given by

$$\mathbf{q}_t + \mathbf{f}'(\mathbf{q})\mathbf{q}_x = 0 \tag{13}$$

where the ij entry of $f'(q)$ is given by

$$f'(q)_{ij} = \frac{\partial f_i}{\partial q_j}. \tag{14}$$

In what follows, we briefly present a general approach for solving equations in quasi-linear form. Details of this approach can be found in [10]. To handle the more general set of equations we use an update described in terms of *fluctuations* $\mathcal{A}^+\Delta Q$ and $\mathcal{A}^-\Delta Q$ given by

$$Q^{n+1}_i = Q^n_i - \frac{\Delta t}{\Delta x}\left(\mathcal{A}^+\Delta Q^n_{i-1/2} + \mathcal{A}^-\Delta Q_{i+1/2}\right) \tag{15}$$

Fluctuations are updates based on the wave structure of the hyperbolic problem and are also obtained by solving Riemann problems. Given eigenvectors r^p and eigenvalues λ^p of the flux Jacobian matrix, or the matrix A, we define characteristic variables α^p by obtaining an eigendecomposition of the jump at cell in $\mathbf{q}$ at cell interfaces. Using the matrix $\mathbf{R} \in R^{m \times m}$ whose p^{th} column is $\mathbf{r}^p$, we define these characteristic variables by solving

$$\mathbf{R}\alpha = Q_i - Q_{i-1} \tag{16}$$

for the vector α, whose entries are the characteristic variables α^p. Using these, we define *waves* $\mathcal{W}^p$ as

$$\mathcal{W}^p = \alpha^p r^p \tag{17}$$

and speeds s^p as the associated eigenvalues λ^p. In general, the eigenvectors and eigenvalues depend on the state vector $\mathbf{q}$, and so for each cell interface $x_{i-1/2}$, one has a different set of waves and speeds. In this case, we use subscripting on the waves $\mathcal{W}^p$ and speeds s^p. With this in mind, fluctuations at cell interface $x_{i-1/2}$ are defined as

$$\begin{aligned} \mathcal{A}^- \Delta Q_{i-1/2} &= \sum_{p=1}^{m} (s_{i-1/2})^- \mathcal{W}^p_{i-1/2} \\ \mathcal{A}^+ \Delta Q_{i+1/2} &= \sum_{p=1}^{m} (s_{i-1/2})^+ \mathcal{W}^p_{i-1/2} \end{aligned} \tag{18}$$

where we have defined

$$(s)^+ = \max(s, 0) \qquad (s)^- = \min(s, 0). \tag{19}$$

For problems in conservation form, the fluctuations $\mathcal{A}^+\Delta Q$ and $\mathcal{A}^-\Delta Q$ define numerical fluxes given by

$$\begin{aligned} F^n_{i-1/2} &\equiv f(Q^n_i) - \mathcal{A}^+ \Delta Q_{i-1/2} \\ &\equiv \mathcal{A}^- \Delta Q_{i-1/2} - f(Q^n_{i-1}). \end{aligned} \tag{20}$$

A *high resolution* scheme can be obtained by including second order correction terms in the update (15). This modified update is given by

$$Q^{n+1}_i = Q^n_i - \frac{\Delta t}{\Delta x}\left(\mathcal{A}^+ \Delta Q^n_{i-1/2} + \mathcal{A}^- \Delta Q_{i+1/2}\right) - \frac{\Delta t}{\Delta x}\left(\widetilde{F}_{i+1/2} - \widetilde{F}_{i-1/2}\right). \tag{21}$$

where the correction terms $\widetilde{F}_{i-1/2}$ are given by

$$\widetilde{F}_{i-1/2} = \frac{1}{2}\sum_{p=1}^{m} |\lambda^p| \left(1 - \frac{\Delta t}{\Delta x}|\lambda^p|\right) \widetilde{\mathcal{W}}^p_{i-1/2} \tag{22}$$

The advantage of this form is that these second order terms can be computed automatically from the wave and speeds returned as a solution to the Riemann problem. Formally, the addition of these terms will lead to a second order accurate scheme for smooth solutions. For problems containing shocks or contact discontinuities, the addition of these terms can lead to spurious oscillations in the solution which we damp with *wave-limiters*. Here, the $\widetilde{}$ on the waves $\mathcal{W}^p_{i-1/2}$ indicates that wave limiters have been applied.

3.2 The Riemann solver for the general detonation problem

For the present detonation problem, we use an approximate solution to the Riemann problem to obtain the desired wave structure. We consider the one-dimensional reactive Euler equations

$$\mathbf{q}_t + \mathbf{f}(\mathbf{q})_x = \mathbf{S}(\mathbf{q}) \tag{23}$$

where $\mathbf{q} = (\rho, \rho u, E, \rho Z)$, the flux function is given by

$$\mathbf{f}(\mathbf{q}) = \begin{pmatrix} \rho u \\ \rho u^2 + p \\ u(E+p) \\ u\rho Z \end{pmatrix} \tag{24}$$

and the source term is defined in (3) or (4). To determine the wave structure, we consider the quasi-linear homogenous form of the above, given by

$$\mathbf{q}_t + \mathbf{f}'(\mathbf{q})\mathbf{q}_x = 0 \tag{25}$$

Using the equation of state given in (6), we can determine the eigen-structure of the flux Jacobian matrix $f'(\mathbf{q})$. The eigenvectors are given by

$$r^1 = \begin{pmatrix} 1 \\ u-c \\ H-uc \\ Z \end{pmatrix} \quad r^2 = \begin{pmatrix} 1 \\ u \\ u^2/2 \\ 0 \end{pmatrix} \quad r^3 = \begin{pmatrix} 1 \\ u+c \\ H+uc \\ Z \end{pmatrix} \quad r^4 = \begin{pmatrix} 0 \\ 0 \\ Q \\ 1 \end{pmatrix} \tag{26}$$

where $H = (E+p)/\rho$ is the enthalpy of the system. The corresponding eigenvalues are given by

$$\lambda^1 = u - c \quad \lambda^2 = u \quad \lambda^3 = u + c \quad \lambda^4 = u. \tag{27}$$

From this characteristic information, we can see that the jump in Z propagates with the speed of the contact discontinuity. Furthermore, this jump induces a jump in energy, also at the contact discontinuity. The details of how to obtain characteristic information for the more general equation of state given in (5), along with multiple species can be found in [11].

To ensure the conservation of the scheme, we must properly choose the value of the state vector $\mathbf{q}$ at which to evaluate the eigenvalues and eigenvectors so that the matrix $\mathbf{A}(\hat{\mathbf{q}}) = \mathbf{f}'(\hat{\mathbf{q}})$ satisfies

$$f(\mathbf{q_r}) - f(\mathbf{q_l}) = \mathbf{A}(\hat{\mathbf{q}})(\mathbf{q}_r - \mathbf{q}_l). \tag{28}$$

Some obvious choices for $\hat{\mathbf{q}}$, such as $\hat{\mathbf{q}} = (\mathbf{q}_r + \mathbf{q}_l)/2$ do not satisfy this property. One special set of values, known as the *Roe-averaged* values, however, do satisfy this property. These values are given by

$$\begin{aligned} \hat{u} &= \frac{\sqrt{u_l}\sqrt{\rho_l} + \sqrt{u_r}\sqrt{\rho_r}}{\sqrt{\rho_r} + \sqrt{\rho_l}} \\ \hat{H} &= \frac{(E_l + p_l)\sqrt{\rho_l} + (E_r + p_r)\sqrt{\rho_r}}{\sqrt{\rho_r} + \sqrt{\rho_l}} \end{aligned} \tag{29}$$

From these values, we can then write the Roe-averaged sound speed as

$$\hat{c} = \sqrt{(\gamma - 1)\left(\hat{H} - \frac{1}{2}\hat{u}^2 - QZ\right)} \tag{30}$$

and obtain waves and speeds which lead to a conservative method. More details about how these values are obtained can be found in [10] and [13].

Finally, the characteristic variables α^p described in (16) can be determined analytically and for the detonation system, are given by

$$\begin{aligned}
\alpha^2 &= (\gamma - 1)(\hat{H} - \hat{u}^2 - QZ)\delta_1 + \hat{u}\delta_2 - \delta_3 + Q\delta_4)/\hat{c}^2 \\
\alpha^3 &= (\delta_2 + (\hat{c} - \hat{u})\delta_1 - \hat{c}\alpha^2)/(2\hat{c}) \\
\alpha^1 &= \delta_1 - \alpha^2 - \alpha^3 \\
\alpha^4 &= \delta_3 - (\alpha_1 + \alpha_3)Z
\end{aligned} \tag{31}$$

These values can be used in (17) to define waves, and along with the eigenvalues (27), one can obtain fluctuations needed to define the cell average update and second order correction terms.

The solution based on the quasi-linear from (1) does not properly take in to account possible rarefaction waves. In the case where the rarefaction waves are either all left going or all right going, the solution structure we obtain leads to a valid numerical solution. However, in the case of transonic rarefactions, one needs to typically include an *entropy* fix to account for the fact that part of the rarefaction is right going, and part is left going. We include a fix proposed by Hymann and Harten and described in [10].

To handle the source term $\mathbf{S}(\mathbf{q})$, we use a fractional step approach, in which we alternate an update to the homogenous system using (9) with an update based on solving the ordinary differential equation

$$\mathbf{q}_t = \mathbf{S}(\mathbf{q}) \tag{32}$$

over the time interval $[t_n\ , t_{n+1}\ ]$. While this operator splitting approach is formally only first order accurate, we have found that it works quite well in practice and is simpler to implement than the second order Strang splitting approach [10].

4 EXTENSIONS TO THE WAVE PROPAGATION ALGORITHM

The above one-dimensional algorithm has been extended to two and three dimensions using either dimensionally split or an unsplit algorithm. The software package CLAWPACK [9] includes a full implementation of a variety of methods for multi-dimensional problems, along with several sample applications.

The extension of the basic wave propagation algorithm to mapped grids are straightforward and has been described in [10] and [5]. Our approach is similar to an unstructured grid approach in that we only require

the locations of the nodes of general quadrilateral or hexahedral meshes rather than analytic formulas for doing grid transformations. One practical advantage of our mapped grid approach is that we can use the same Riemann solver for both mapped and non-mapped problems. Furthermore, we have written several routines which automate the process of computing and accessing the metric terms needed to implement our algorithms in two and three dimensions. We have performed several numerical tests of this approach and have found that the numerical accuracy of the scheme is essentially the same as that on a uniform Cartesian grid, at least for reasonably smooth mappings. In particular, our mapped grid approach works well even on non-smooth meshes [5].

The mapped grid algorithms we present here can be naturally extended to solve problems on a nested hierarchy of adaptively refined grids. The advantage of adaptive mesh refinement, or AMR, is that one reserves computational effort only for those computational regions where the solution is of interest. To take advantage of AMR, we have built our single grid routines into CHOMBO, a general AMR infrastructure developed at Lawrence Berkeley Laboratory [6]. Many of our simulations have been done using the resulting software, CHOMBOCLAW [3]. CHOMBOCLAW is freely available, and runs on a variety of platforms, including distributed computing environments.

A second software package, AMRCLAW is also available for using AMR technology with wave propagation algorithms [2].

5 NUMERICAL RESULTS

We first verify that we have implemented the Riemann solver correctly by solving a one-dimensional detonation problem and comparing our results with the exact solution obtained from Chapman-Jouguet theory. We use a $\tau = 0.025$, and set up initial conditions so that the speed of the moving front is exactly equal to 1. We also use this solution to demonstrate the need for fine-grid resolution to obtain accurate peak-overpressures. In Figure 1, we show plots of the pressure solved on a 100 and 800 grid points and compare these results with the exact solution. As expected, the solution computed on 800 grid points comes much closer to achieving the peak over-pressures than the coarse grid solution. This confirms the need for refinement, at least locally, to obtain accurate measurements of pressure loads on containment structures.

To validate the results, we have also done some initial validation tests with experimental results obtained from the Frauenhofer Institute [12]. In that comparison, our results agreed well with the experimental data on peak-overpressures in a spherically symmetric expanding detonation front in a 30% hydrogen-air mixture [4].

5.1 Two dimensional results

To model the containment structure, we use a grid mappings based on ideas from [5]. Figure 3 shows an example of the curvilinear mesh we used for our present two-dimensional calculations. For this example, we assume that we have a homogenous 30% hydrogen mixture and that there are no obstacles inside the

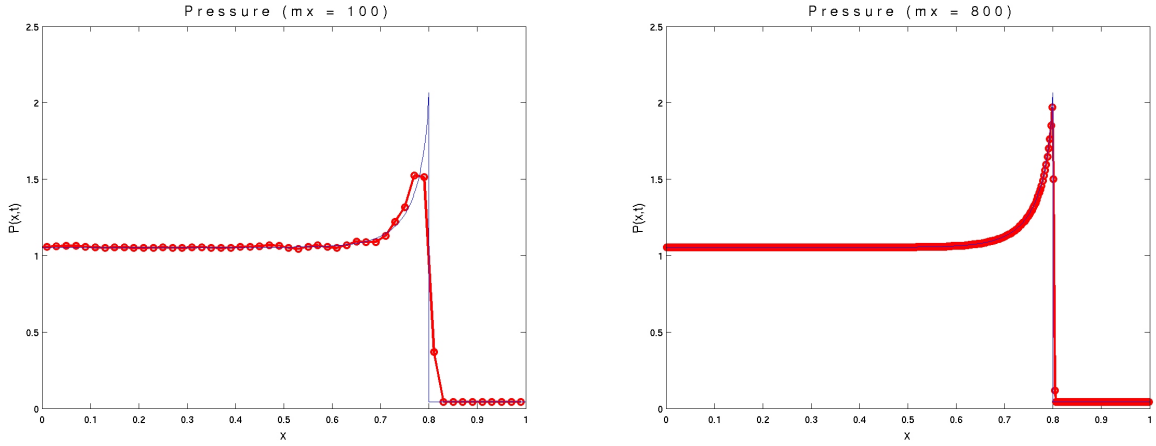

Figure 1. Comparison of the one-dimensional ZND solution to the pressure at two different levels of grid refinement. In each plot, the solution computed using the wave-propagation algorithm is shown using 'o's. The solid line is the semi-analytic traveling wave solution. In the left plot, the solution is computed on 100 grid points, and the right, on 800 grid points.

containment. We initialize the combustion process inside a small circular region using values computed from Chapman-Jouguet theory. These values are given in Table I. Other values are $T_{ign} = 757K^0$. On the boundaries of the containment, we impose solid wall (or reflecting) boundary conditions.

Table I. Initial values for detonation problem

	Unburned region	Burned region
Pressure (Pa)	99700	2.5×10^6
Density (kg/m^3)	0.875	1.48
Temperature (K^o)	285	5005
Hydrogen concentration	30%	0.7%

To capture potential pressure peaks accurately without resolving the mesh everywhere, we use two levels of mesh refinement, with a refinement ratio of four between the two levels. This results in an effective mesh resolution on the finest level of 360×720. A region of the mesh is tagged for refinement if the jump between mesh cells in any of the four conserved quantities exceeds a specified threshold value.

In Figure 2, we show the pressure contours that result from the detonation shown in the left plot. In Figure 3, we plot the values of the pressure along the perimeter of the containment. From this plot, it is clear that the pressure along the containment walls can exceed by several times the pressure values obtained in free

space.

5.2 Three dimensional results

In this example, we use the same initial conditions as for the two dimensional example. To model the containment structure, we again use grids based on ideas proposed in [5], and so we can model the entire containment with a single grid. In Figure 4, we show the results at a single time step of this calculation.

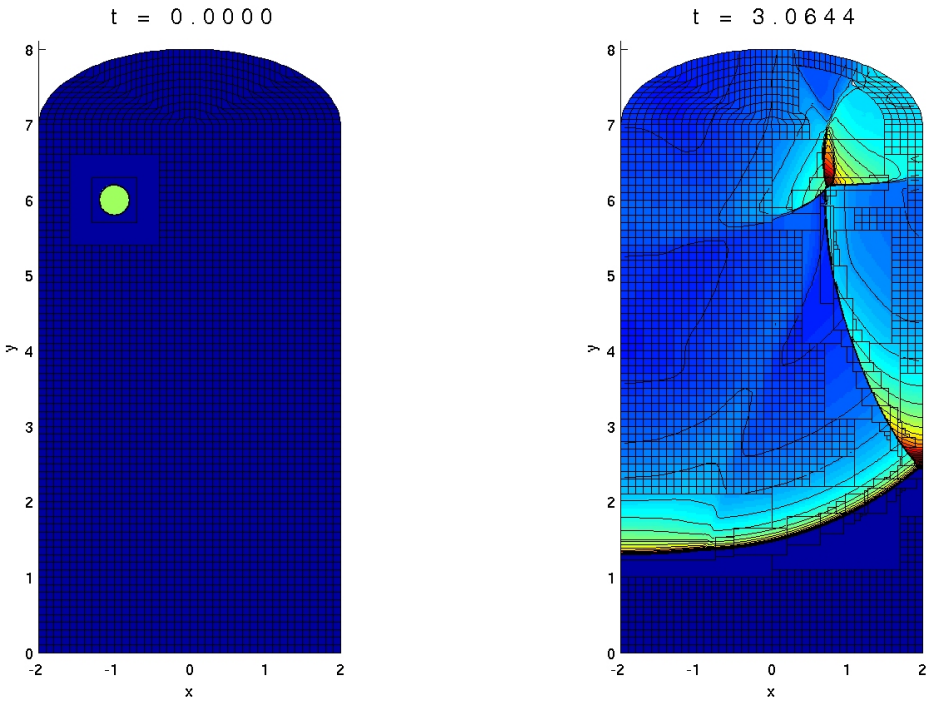

Figure 2. The left plot shows a coarsened single grid version of the computational mesh used for the two-dimensional calculations. The circular region at $(-10, 50)$ is the source of the initial detonation. The right plot shows the contours of pressure at time $t = 0.0188$ resulting from the detonation. The boxes in the right plot are the grid patches that have been refined by a factor of four from the background coarse mesh. Note that the z-axis unit is 10 meters.

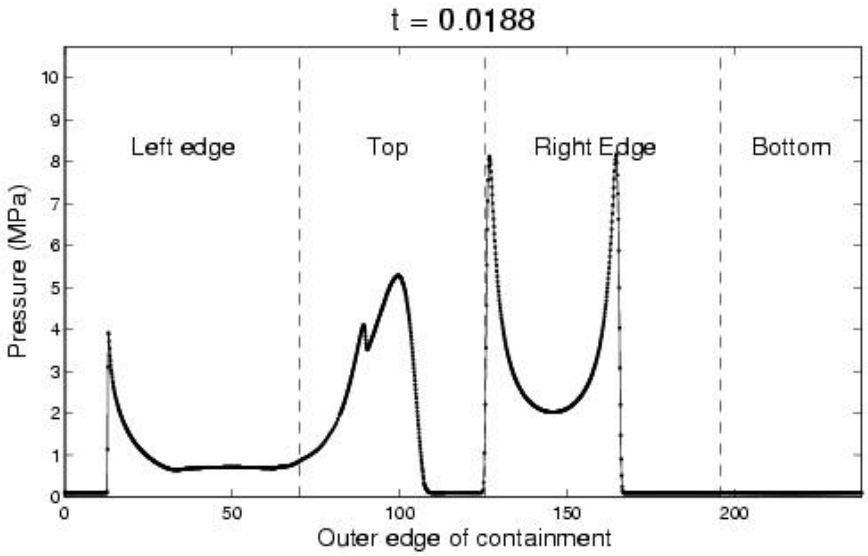

Figure 3. Pressure along the perimeter of the containment structure. The curve starts at the lower left corner, and preceeds clockwise around the perimeter of the structure.

6 CONCLUSIONS AND FUTURE WORK

The computations we have presented illustrate at least one approach to obtaining detailed temporal and spatial information about blast loading on a two- and three-dimensional containment structure. These results are very preliminary in that we have not considered detailed ignition mechanisms or deflagrations in heterogenous hydrogen-air mixtures. Furthermore our interior containment geometry is greatly simplified, and as such, does not likely capture important geometric effects due to internal structures. However, we believe that even these preliminary results could be used, for example, in conjunction with the results presented in [1] to assess the strength of the containment walls. Currently, work is underway to handle the more general equation of state given in (5). Also, we are currently implementing a Cartesian grid embedded boundary method for handling more complex geometry [7].

REFERENCES

[1] A.K.Panday, R. Kumar, D.K.Paul, and D.N.Trikha. Non-linear response of reinforced concrete containment structure under blast loading. *Nuclear Engineering and Design*, 236:993–1002, 2006.

[2] M. J. Berger and R. J. LeVeque. Adaptive mesh refinement using wave-propagation algorithms for hyperbolic systems. *SIAM J. Numer. Anal.*, 35:2298–2316, 1998.

[3] D. Calhoun. ChomboClaw User's Guide, Version 1.0. Technical report, Lawrence Berkeley Laboratory, 2005. In preparation.

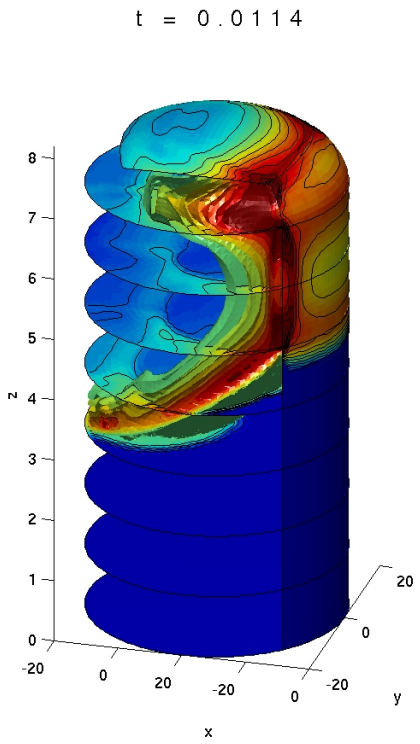

Figure 4. Three dimensional simulation of a potential hydrogen explosion in a containment building.

[4] D. Calhoun. Simulating detonations using adaptively refined, mapped cartesian grids. Technical report, Commissiariat á l'Energie Atomique, Direction de l'Energie Nucleaire, 2007. in revision.

[5] D. A. Calhoun, C. Helzel, and R. J. LeVeque. Logically rectangular grids and finite volume methods for PDEs in circular and spherical domains. *submitted*, 2006.

[6] CHOMBO. Applied Numerical Algorithms Group, Lawrence Berkeley Laboratory, CA, USA. Available on the Web at `http://seesar.lbl.gov/anag/chombo/`.

[7] P. Colella, D. T. Graves, B. J. Keen, and D. Modiano. A Cartesian Grid Embedded Boundary Method for Hyperbolic Conservation Laws. Technical report, Lawrence Berkeley National Laboratory, 2004. LBNL-56420.

[8] A. A. Efimenko and S. B. Dorofev. CREBCOM code system for description of gaseous combustion. *Journal of Loss Prevention in the Process Industries*, 14:575–581, 2001.

[9] R. J. LeVeque. CLAWPACK software. `http://www.amath.washington.edu/~claw`.

[10] R. J. LeVeque. *Finite Volume Methods for Hyperbolic Problems*. Cambridge University Press, 2002.

[11] S. Osher R. Fedkiw, B. Merriman. Numerical methods for a mixture of thermally perfect and/or calorically perfect gaseous species with chemical reactions. *jcp*, 132:175–190, 1997.

[12] A. Silde and I. Lindholm. On detonation dynamics in hydrogen-air-steam mixtures: Theory and application to olkiluoto reactor building. Technical Report NKS-9, VTT Energy, Finland, 2000. ISBN 87-7893-058-8; Available on the Web at URL `www.nks.org`.

[13] E.F. Toro. *Riemann Solvers and Numerical Methods for Fluid Dynamics*. Springer-Verlag, second edition, June 1999. 624 pages.